Blade Design Trade-Offs Using Low-Lift Airfoils for Stall-Regulated HAWTs

P. Giguère*

M. S. Selig†

University of Illinois at Urbana-Champaign
Urbana, IL 61801

J. L. Tangler‡
National Renewable Energy Laboratory
Golden, CO 80401

A systematic blade design study was conducted to explore the trade-offs in using low-lift airfoils for a 750-kilowatt stall-regulated wind turbine. Tip-region airfoils having a maximum-lift coefficient ranging from 0.7–1.2 were considered in this study, with the main objective of identifying the practical lower limit for the maximum-lift coefficient. Blades were optimized for both maximum annual energy production and minimum cost of energy using a method that takes into account aerodynamic and structural considerations. The results indicate that the effect of the maximum-lift coefficient on the cost of energy is small with a slight advantage to the highest maximum lift coefficient case considered in this study. As a consequence, higher maximum lift coefficient airfoils for the tip-region of the blade become more desirable as machine size increases, provided the airfoils yield acceptable stall characteristics. The conclusions are applicable to large wind turbines that use passive or active stall to regulate peak power.

1 Introduction

The use of aerodynamic stall is a common means of regulating peak power for horizontal axis wind turbines (HAWTs) operating at constant speed. Stall regulation can be performed either actively (pitch control) or passively (fixed pitch), the latter being the more popular approach. For both of these approaches, the stall characteristics of the airfoils used over the tip region of the blades are important because they strongly affect the dynamics of the rotor, and thus the structural design of the blades. Reducing blade dynamic excitations, such as stall-induced vibrations, can be achieved using airfoils having a gentle stall, which typically have a low maximum-lift coefficient ($c_{l,\max}$), i.e., low-lift airfoils. In contrast, high-lift airfoils often have an abrupt or hard stall that is characterized by a rather large loss in lift and negative lift-curve slope. As a result, high-lift airfoils increase blade dynamic excitations as compared with low-lift airfoils. The use of high-lift airfoils, however, is beneficial for minimizing blade solidity and enhancing starting torque. Also, for a given amount of laminar flow, high-lift airfoils are more efficient (higher lift-to-drag ratio) than airfoils with a low $c_{l,\max}$. Therefore, there are competing design trade-offs in selecting the lift range of the airfoils for a particular rotor.

The trade-offs between low-lift and high-lift airfoils for stall-regulated HAWTs have been recognized for some time now. Since 1984, the National Renewable Energy Laboratory (NREL), in collaboration with Airfoils Inc., have developed over 10 airfoil families specifically for wind turbines. Most tip-region airfoils have a low $c_{l,\max}$, in the range of 0.9–1.2, while the root airfoils have a higher $c_{l,\max}$ (Tangler and Somers, 1985, 1987, 1995). Another important characteristic of the NREL airfoils is that their $c_{l,\max}$ is less sensitive to roughness effects as compared with airfoils that were designed for aircraft applications and used on wind turbines (Tangler and Somers, 1995). Blades for both experimental and commercial wind turbines have successfully used the NREL airfoils (Tangler et al., 1992, 1994; Huyer et al., 1996). The approach of using a high-lift airfoil for the inboard part of the blade and low-lift airfoils for the tip region has also been reiterated in a recent report from Risø (Petersen et al., 1998). More precisely, this report states that high-lift airfoils are desirable inboard to obtain a slender blade and low lift-airfoils should be preferred outboard to minimize negative aerodynamic damping.

Even though the importance of using low-lift airfoils in the tip region has been recognized (Tangler and Somers, 1995; Petersen et al., 1998), it is unclear if there is merit in considering airfoils having a lower $c_{l,\max}$ than that of the NREL airfoils. Accordingly, the present research effort focused on identifying the practical lower limit of the maximum-lift coefficient within the range of 0.7–1.2 for airfoils tailored for stall-regulated wind turbines. Another objective was to investigate the effects of increasing swept area by reducing $c_{l,\max}$ in the blade-tip region. To carry out those two objectives, a method for rotor optimization that takes into account both aerodynamic and structural considerations was developed. The blade design method, which is described in Section 2, was used to perform a systematic blade design trade-off study for a 750-kilowatt (kW) stall-regulated HAWT. The results of this study are presented and discussed in Section 3. Section 4 provides the conclusions, which are applicable to large wind turbines that use passive or active stall to regulate peak power.

2 Blade Design Method

The blade design approach section is subdivided into six subsections, namely: (1) design approach, (2) design constraints, (3) annual energy production computation, (4) cost of energy computation, (5) airfoil data, (6) case matrix and optimization cases.

2.1 Design Approach. The blade design trade-off study was performed using the computer program PROPGA (Selig and Coverstone-Carroll, 1996; Giguère and Selig, 1997), which is a genetic algorithm based optimization method for the blade geometry of HAWTs. In brief, PROPGA mimics Darwin's theory of the survival of the fittest over a population of candidate blade shapes that evolves from one generation to the next. Blade designs having a large fitness according to the objective function for the optimization process have a larger probability to "reproduce" in creating the new generations compared with those with a small fitness value. A binary string represents each candidate blade geometry, and the reproduction process involves crossover and mutation operators.

---

* Graduate Research Assistant, Aeronautical and Astronautical Engineering Department.
† Associate Professor, Aeronautical and Astronautical Engineering Department.
‡ Senior Scientist, National Wind Technology Center.

The results of this paper were presented at the ASME Wind Energy Symposium, Reno, NV, January 11–14, 1999.
Contributed by the Solar Energy Division of The American Society of Mechanical Engineers for publication in the ASME JOURNAL OF SOLAR ENERGY ENGINEERING. Manuscript received by the ASME Solar Energy Division, Mar. 1999; final revision, Nov. 1999. Associate Technical Editor: P. S. Veers.

In this work, two objective functions were considered: maximum annual energy production (AEP) and minimum cost of energy (COE). For the optimization for maximum AEP, PROPGA was used to determine the optimum chord and twist distributions as well as the blade pitch for a given airfoil family. The chord and twist/pitch were optimized at four radial stations (15%, 40%, 75%, and 95% radius) and a cubic spline was used to obtain the chord and twist values at each blade segment. In optimizing for minimum COE, PROPGA provided the optimum rotor diameter in addition to the optimum chord, twist, and pitch. The computer program PROPID (Selig and Tangler, 1996; Giguère and Selig, 1997), which is an inverse design method for HAWTs based on the PROP code (Wilson and Walker, 1974; Hibbs and Radkey, 1983), was used to analyze the rotor performance of the candidate blade designs. The AEP was computed by PROPID while the COE computations were performed by PROPGA.

The following PROPGA and PROPID settings were used:

- Population size of 252
- String length of 56 bits for AEP optimization and 63 bits for COE optimization (7 bits per parameter)
- A total of 25 generations
- Tournament selection
- Uniform crossover with a 50% probability
- Mutation rate of 1%
- Elitism on (best blade design of one generation is copied as is into the subsequent generation)
- Niching on all parameters (Giguère and Selig, 1997)
- 10 blade segments
- Prandtl tip-loss model
- Swirl on
- Corrigan stall-delay model (Tangler and Selig, 1997)
- Sea-level atmospheric conditions

2.2 Design Constraints. The trade-off study was conducted for a three-blade, upwind, fixed-pitch, 750-kW HAWT having a baseline rotor diameter of 44 m. In the optimization process, the inverse design capability of PROPID was used to ensure a rated power of 750 kW by iterating on blade pitch. For noise considerations, the tip speed was fixed at 62 m/s, which corresponds to 27 revolutions per minute (rpm) for the baseline rotor diameter. Therefore, the rpm was adjusted according to the rotor diameter for the case of the optimization for minimum COE. Airfoil families made up of three airfoils (root, primary, and tip airfoils) were considered. The distribution of these airfoils along the blade and their respective thickness was fixed, i.e., root airfoil (24% thick) up to 40% radius, primary airfoil (21% thick) at 75% radius, and tip airfoil (16% thick) at 95% radius. This airfoil distribution is that of the NREL thick-airfoil families, which were designed primarily for stall-regulated HAWTs (Tangler and Somers, 1995).

2.3 Annual Energy Production Computation. PROPID generated a power curve from the cut-in to cut-out wind speed of 25 m/s, with a 1 m/s increment. The power curves reflected the enhanced lift inboard of the blade owing to stall delay as modeled with the Corrigan stall-delay model (Tangler and Selig, 1997). A Rayleigh wind speed distribution was used in computing the AEP. Two wind classes of the International Electrotechnical Commission (IEC) were considered, namely class II and IV having an average wind speed of 8.5 m/s and 6 m/s, respectively. No losses were considered, and thus the AEP values presented in this paper represent the gross output.

2.4 Cost of Energy Computation. The COE was calculated using the following expression:

$$COE = \frac{(TC + BOS)}{AEP} FCR + O \& M \qquad (1)$$

In this equation, the turbine cost TC was based on the blade cost BC and the assumption that the blades represent 20% of the total turbine cost. Two approaches were used to determined the turbine cost, i.e., $TC = 5 \cdot BC$ or $TC = BC + RC$ where RC is the remaining turbine cost, which was fixed and taken as four times the blade cost of a baseline rotor. These two approaches represent extremes in estimating the impact of the rotor design on the overall TC. The first approach suggests a linear impact of the rotor on the cost of the other components. In contrast, the second approach neglects that impact, and thus is more appropriate when comparing results for a fixed rated power and rotor diameter. Results for both of these approaches to compute the TC are presented, thereby giving trends for both extremes in estimating the impact of the rotor design on the other turbine components. The blade cost was determined according to a weight estimate for E-glass using a price of \$20/kg, which includes labor, overhead, and profit. For the balance of station BOS a cost of \$200/kW was considered, thus fixing the BOS to \$150,000 for a 750-kW turbine. The fixed charge rate FCR was 11% and a 98% availability was applied to the annual energy production AEP. Finally, a fixed cost of \$0.01/kWh was used for operation and maintenance O & M. The value of the blade cost being 20% of the total turbine cost and the BOS, FCR, and O & M costs were obtained from discussions with NREL personnel.

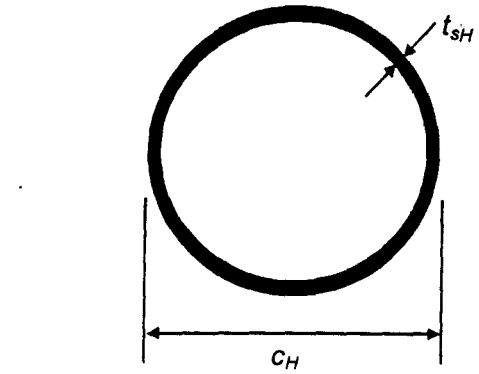

Fig. 1(*a*)

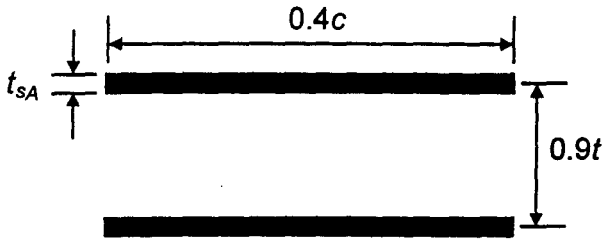

Fig. 1(*b*)

Fig. 1 Modeling of the (*a*) hub and (*b*) the airfoil section for estimating the blade weight

In estimating the blade weight, the hub (5% of blade span) was modeled as a tube, and the airfoil section was modeled as an I-beam without a shear web, as shown in Fig. 1. This modeling approach has been used in other wind turbine optimization work (Fuglsang and Madsen, 1995). The hub skin thickness is t_{sH} and the diameter of the hub is d_H. For the airfoil section at a given blade segment, t_{sA} is the skin thickness, c is the chord, and t is the physical thickness. It is important to note that in this modeling of the airfoil section, the skin as shown in Fig. 1(*b*) is not the actual spar but rather a representation of the overall skin thickness that is carrying the load.

The procedure for estimating the blade weight began with the computation of the flap-bending loads at each blade segment from the thrust distribution for a given load condition. Although there are many design load cases in the IEC standards (International Electrotechnical Commission, 1998), the parked rotor in a 50-year extreme wind design situation (hurricane condition) was consid-

ered in this study because of the inverse relationship between the $c_{l,max}$ of the airfoils used and the resulting blade area. The ultimate flap-bending loads were computed for either an IEC wind class II (59.5 m/s) or IV (42 m/s) with the blades fully exposed to the wind (fixed-pitch turbines), and the IEC partial safety factor for loads (load factor) of 1.35 was applied to the static flap-bending loads. Using the static flap-bending load M for a given blade segment or radial position r, the required moment of inertia I for that segment to match a prescribed stress level σ_p along the blade was computed according to Eq. 2. The skin thickness t in Eq. 2 represents either that of the hub or the airfoil section depending on the given blade segment.

$$I(r) = \frac{M(r)[t(r)/2]}{\sigma_p(r)} \tag{2}$$

The prescribed stress level was the same for each blade segment, and E-glass was the material of choice. Results from structural static-tests to failure of full-scale composite blades were used to determine a representative value for the ultimate strength of E-glass (Sutherland et al., 1994; Musial, 1999). The NREL thin airfoil 7.9-m blade failed at a strain level of approximately 5000 $\mu\epsilon$ (Sutherland et al., 1994). This result is also supported by unpublished data from similar tests conducted with several blades for the U.S. Windpower 56-100 wind turbine (Musial, 1999). For E-glass (Mandell and Samborsky, 1997), a tensile elastic modulus of 28 GPa ($\approx 4 \times 10^6$ psi) was used resulting in an ultimate strength of 140 MPa ($\approx 20 \times 10^3$ psi). Partial safety factors for the material were applied to account for creep and temperature effects. Such safety factors are not given by the IEC standards, and those imposed by Germanisher Lloyd were used, namely 1.5 for creep, and 1.1 for temperature effects, giving an overall partial safety factor for the material of 1.65. Safety factors for manufacturing and heat treatment effects were not used as the test results from which the ultimate strength was derived already account for these effects. Furthermore, the general safety factor of 1.35 of Germanisher Lloyd was not considered as it is already accounted for with the IEC load factor, and the IEC partial safety factor for consequence of failure for an ultimate strength analysis is 1.0. Therefore, the prescribed stress level at each blade segment was 84.85 MPa (140 MPa/1.65).

Given the required moment of inertia at each blade segment, the required skin thickness was then determined from Eqs. 3 and 4 for the hub and airfoil sections, respectively.

$$t_{sH} = \frac{I_H}{\pi\left(\frac{d_H^3}{8}\right)} \tag{3}$$

$$t_{sA}(r) = \frac{I(r)}{(81/500)ct^2} \tag{4}$$

Note that the contribution of the skin about its own rotational axis was neglected in the expression of the moment of inertia of the airfoil section because it is much smaller than the inertia resulting from the distance of the material from the neutral axis. Also, the minimum skin thickness was set to 5 mm.

From the skin thickness distribution along the blade obtained from Eqs. 3 and 4, the blade cross-sectional area at each segment was calculated according to Fig. 1. Realistically, not all the skin of the blade is carrying the load. Consequently, the minimum skin thickness was applied to the airfoil perimeter along the leading and trailing edges. The blade material volume was then computed from linear extrapolations of the local cross-sectional area of each of the 10 blade segments. Finally, the blade weight was obtained using a density of 2000 kg/m^3, which is representative of E-glass. Figure 2 summarizes the process of computing COE.

2.5 Airfoil Data. Because of the limited amount of aerodynamic data on low $c_{l,max}$ airfoils designed for large HAWTs and

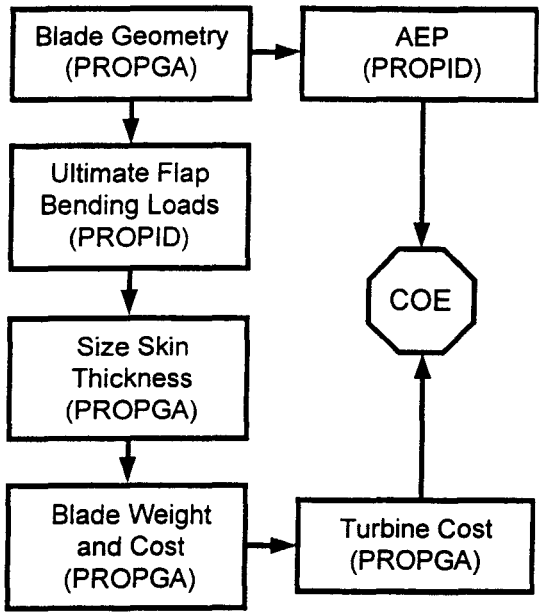

Fig. 2 Flow chart outlining the different steps to compute COE

short of designing airfoils specifically for this work, synthesized airfoil data covering a $c_{l,max}$ range of 0.7–1.2 was generated for this study. This synthesized airfoil data was based on Eppler code (Eppler and Somers, 1980) predictions for the NREL S818 (root, $c_{l,max}$ of 1.4), S827 (primary, $c_{l,max}$ of 1.0), and S828 (tip, $c_{l,max}$ of 0.9) airfoils, which form one of the NREL thick-airfoil families for extra-large blades (Tangler and Somers, 1995) that is referred to here as the baseline airfoil family. Data was synthesized for a total of five airfoil families including the baseline family. The S818 was used as the common root airfoil for all families. The primary and tip airfoils had $c_{l,max}$ between 0.8–1.2 and 0.7–1.1, respectively. Figure 3 presents the synthesized data for the five primary airfoils.

The method used to obtain the synthesized data from the lift and drag coefficients (c_l and c_d) of the S827 and S828 was to add a c_l increment (Δc_l) to attain the desired $c_{l,max}$ and modify the c_d values using a scale factor, which depended on the Δc_l. More precisely, the c_d scale factor was set to 1.0 for negative Δc_l while values of 1.0375 and 1.075 were used for Δc_l of 0.1 and 0.2, respectively. These c_d scale factors were derived from Eppler predictions for other NREL airfoils, namely the S816, S817, and S829, which were also designed for extra-large blades (Tangler and Somers, 1995). Because of the shortcomings of the Eppler code and other computational airfoil analysis programs in accurately predicting $c_{l,max}$ and data beyond stall, results from the Delft wind tunnel tests for the S809 (Somers, 1997a) and S814 (Somers, 1997b) airfoils were used to extend the data into stall. Therefore, the root S818 airfoil had a harder stall than that for the primary and tip airfoils, which used the S809 stall characteristics. The roughness effects were not modeled in this study because a recent report indicated that roughness effects on aft-cambered NREL airfoils are mainly driven by airfoil thickness and not $c_{l,max}$ (Tangler and Somers, 1999). In this study, the airfoil thickness distribution is the same for all airfoil families. Therefore, roughness losses can be considered to be essentially the same owing to the similarity in the airfoil characteristics.

Although not presented in this paper, the airfoil data covered the Reynolds number range of 2–5 $\times 10^6$ with an increment of 1 $\times 10^6$. Furthermore, the Corrigan stall-delay model (Tangler and Selig, 1997) was used to modify the two-dimensional data for three-dimensional and rotational effects. Linear interpolation was used between airfoil data files for stations where there is a blend of airfoils. The use of these airfoil data files allows for the interpolation/extrapolation of the data with Reynolds numbers. Linear interpolation is used for lift, and logarithmic interpolation is

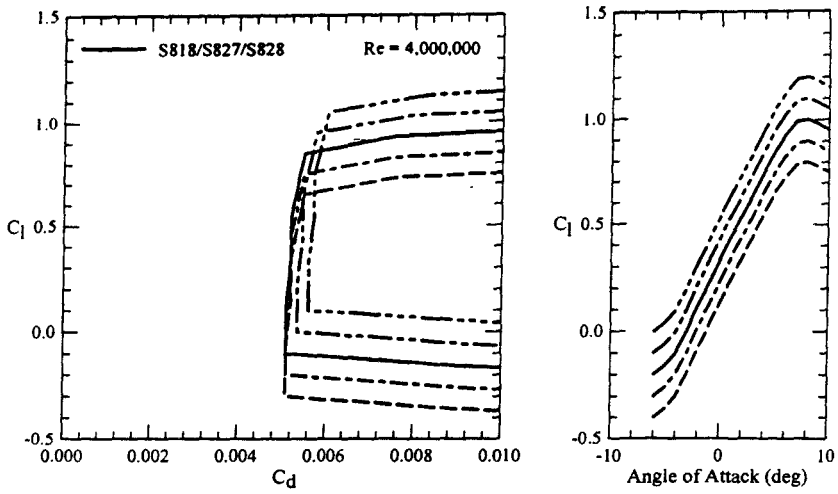

Fig. 3 Synthesized airfoil data for the primary airfoils based on the NREL S827 airfoil

used for drag to accurately represent the airfoil characteristics. Note that extrapolation of the data is not performed for Reynolds numbers smaller than the minimum Reynolds number (2×10^6) in each airfoil data file.

2.6 Case Matrix and Optimization Cases. The case matrix used for this study is shown in Table 1. A total of five design cases were considered representing the five airfoil families. The airfoil names starting with "75" represent the primary airfoils that are located at 75% radius while those beginning with "95" (95% radius) are the tip airfoils. Again, the root airfoil was the same for all airfoil families, and thus it has been omitted in Table 1. Each airfoil name has a two-digit number by the "75" or the "95" representing the $c_{l,\max}$ of that airfoil. Therefore, airfoil 75-08 is a primary airfoil with a $c_{l,\max}$ of 0.8. All cases or airfoil families have a $c_{l,\max}$ that decreases from root to tip, in a similar fashion to the NREL airfoil families. Case 10-09 represents the baseline airfoil family from which the baseline blade cost needed to compute the turbine cost was determined.

As mentioned in subsection 2.1, optimizations were performed for both maximum AEP and minimum COE, which represent the two optimization cases. The optimizations for maximum AEP were performed for IEC wind class II under two scenarios. In the first scenario, the rotor diameter was fixed to the baseline value of 44 m. For the second scenario, the rotor diameter was increased with decreasing $c_{l,\max}$. Table 2 indicates the increase in diameter and corresponding increase in swept area for each of the five cases. The optimization for minimum COE, for which the rotor diameter was a free variable, was carried out for IEC wind classes II and IV. Overall, a total of 60 PROPGA runs were performed in this study.

3 Results and Discussion

This section presents the results for AEP and COE for each of the five cases shown in the case matrix (see Table 1). In addition, the chord distribution for each case is depicted. The results for the two optimization cases are presented and discussed separately.

Table 1 Five design cases representing five airfoil families

Airfoils	95-07	95-08	95-09	95-10	95-11
75-08	c08-07	–	–	–	–
75-09	–	c09-08	–	–	–
75-10	–	–	c10-09	–	–
75-11	–	–	–	c11-10	–
75-12	–	–	–	–	c12-11

3.1 Optimization for Maximum AEP. Figure 4 shows the AEP for the five design cases. Clearly, the AEP is basically the same for all cases when the rotor diameter was fixed (maximum difference of 0.3%). As expected, the AEP scales with the increase in rotor diameter, with a maximum difference of 3% in AEP.

The blades that were optimized for maximum AEP were also analyzed for loads and cost to provide COE estimates, which are presented in Figs. 5 and 6. Both of these figures, which present results for the case of a fixed rotor diameter and that with increasing rotor diameter with decreasing $c_{l,\max}$, show results having similar trends. A linear scaling of the blade cost to determine the turbine cost indicates a small advantage to the highest $c_{l,\max}$ case. In contrast, when the impact of the blade design on the other turbine components is neglected, all cases yield the same COE. For the case of a fixed rotor diameter, more weight should be given to the trend for the latter approach to compute the turbine cost (TC =

Table 2 The increase in diameter and corresponding increase in swept area for each of the five cases

Case	Diameter (m)	% Incr.	Swept Area (m^2)	% Incr.
c08-07	23.10	5.0	1676.4	10.3
c09-08	22.88	4.0	1644.6	8.2
c10-09	22.66	3.0	1613.1	6.1
c11-10	22.44	2.0	1582.0	4.0
c12-11	22.22	1.0	1551.1	2.0

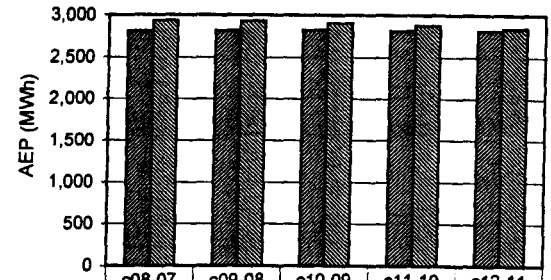

	c08-07	c09-08	c10-09	c11-10	c12-11
Fixed Rotor Dia. (44 m)	2807.0	2814.4	2820.5	2816.1	2813.6
Increasing Rotor Dia. (5%,4%,3%,2%,1%)	2936.1	2927.8	2902.4	2874.0	2842.3

Fig. 4 Annual energy production for the cases considered in the optimization for maximum AEP (the increase in rotor diameter is 5% for c08-07, 4% for c09-08, 3% for c10-09, 2% for c11-10, and 1% for c12-11)

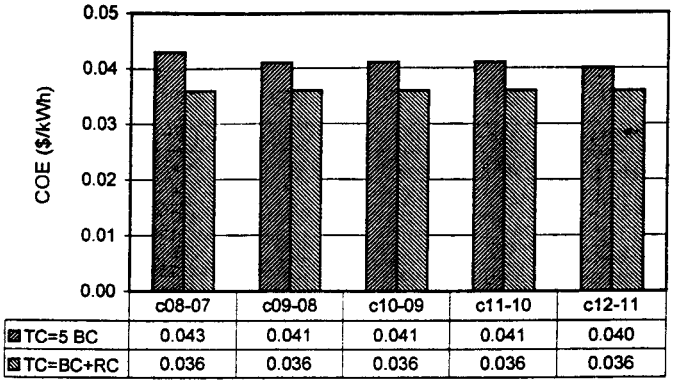

	c08-07	c09-08	c10-09	c11-10	c12-11
TC=5 BC	0.043	0.041	0.041	0.041	0.040
TC=BC+RC	0.036	0.036	0.036	0.036	0.036

Fig. 5 Cost of energy for the optimization for maximum AEP with a fixed rotor diameter II using both methods considered to compute the total turbine cost

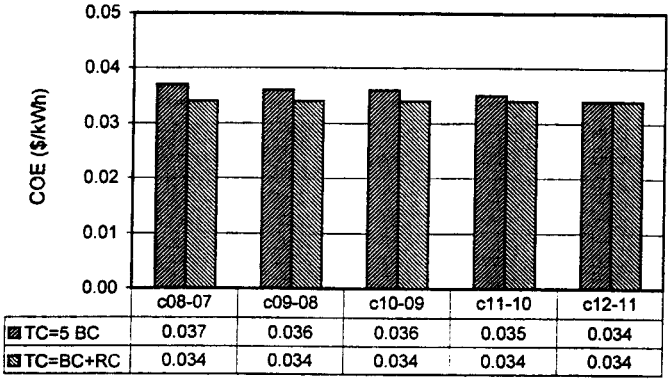

	c08-07	c09-08	c10-09	c11-10	c12-11
TC=5 BC	0.037	0.036	0.036	0.035	0.034
TC=BC+RC	0.034	0.034	0.034	0.034	0.034

Fig. 8 Cost of energy for the optimization for minimum COE and IEC wind class II using both methods considered to compute the total turbine cost

$TC + RC$) because the rotor design has a small impact on the remaining turbine cost when the rated power and rotor diameter are fixed. The opposite apply for the case of increasing rotor diameter with decreasing $c_{l,\max}$.

The lower COE of the higher $c_{l,\max}$ cases for the case of linear scaling between blade and turbine cost can be explained by the chord distributions depicted in Fig. 7. For a given rated power, the blade area is inversely proportional to the $c_{l,\max}$ of the airfoils used. Therefore, the lower $c_{l,\max}$ cases resulted in broad outboard chord lengths, thereby resulting in higher blade loads under the 50-year extreme wind parked rotor condition and larger overall cost of the turbine. These differences in chord distributions have no effect on the COE when the blade cost has no impact on the remaining turbine cost. The inboard chord distributions were mostly similar because the same root airfoil was used.

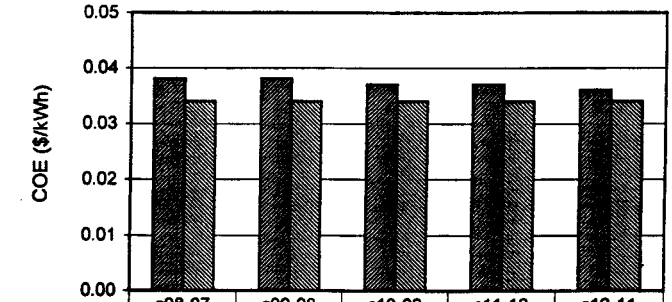

	c08-07	c09-08	c10-09	c11-10	c12-11
TC=5 BC	0.038	0.038	0.037	0.037	0.036
TC=BC+RC	0.034	0.034	0.034	0.034	0.034

Fig. 6 Cost of energy for the optimization for maximum AEP with increasing rotor diameter with decreasing $c_{l,\max}$ II using both methods considered to compute the total turbine cost (the increase in rotor diameter is 5% for c08-07, 4% for c09-08, 3% for c10-09, 2% for c11-10, and 1% for c12-11)

3.2 Optimization for Minimum COE. The COE results for the blades optimized for minimum COE and an IEC wind class II are presented in Fig. 8. The results of this figure yield similar trends than those of Figs. 5 and 6, and those obtained for the IEC wind class IV, which are not shown. With the rotor diameter as a free variable in the optimization for minimum COE, more weight should be given to the results obtained using the linear scaling approach of the blade cost to the turbine cost ($TC = 5BC$). Therefore, there is a trend of lower COE with increasing $c_{l,\max}$, but that advantage remains small.

Figure 9 depicts the chord distributions for the case of a linear scaling between blade and turbine cost. Results for both an IEC wind class II and IV are shown. The blades designed for an IEC wind class II are more similar to each other compared with those designed for the IEC wind class IV. Consequently, the parked rotor

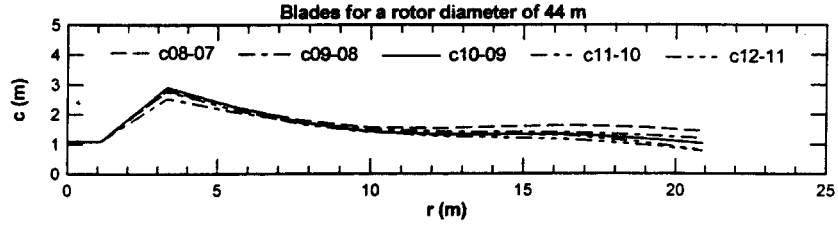

Fig. 7(*a*)

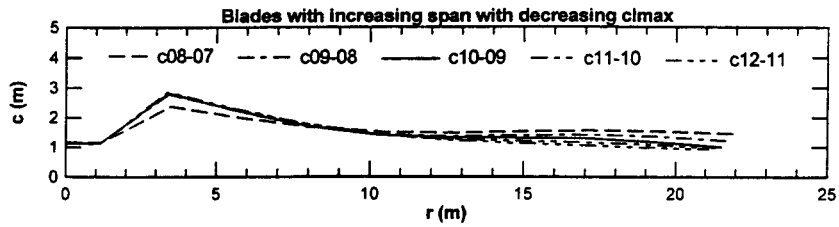

Fig. 7(*b*)

Fig. 7 Chord distributions for the cases considered in the optimization for maximum AEP: (*a*) fixed rotor diameter and (*b*) increasing blade span with decreasing $c_{l,\max}$

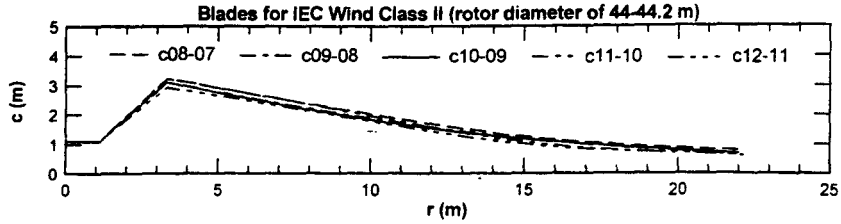

Fig. 9(*a*)

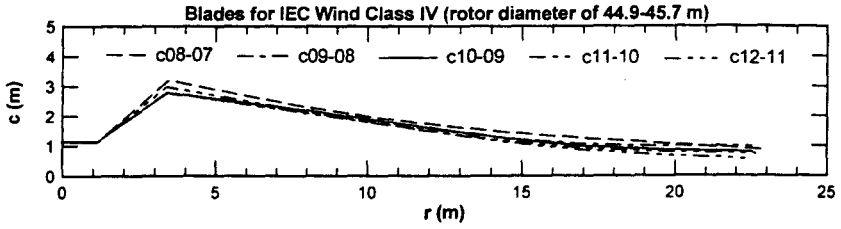

Fig. 9(*b*)

Fig. 9 Chord distributions for the cases considered in the optimization for minimum COE: (*a*) IEC wind class II and (*b*) IEC wind class IV

in a 50-year extreme wind condition clearly drove the blade design, which explains the rather large inboard chords given the fixed airfoil thickness distribution. The inboard chords could be reduced to more practical values using a thicker root airfoil at the cost of increased roughness losses (Tangler and Somers, 1999). The ultimate load condition was less severe for the IEC wind class IV, and thus the differences in chord distributions were larger in that case. PROPGA found that slightly larger rotor diameters than the baseline (44.9–45.7 m) were optimum for IEC wind class IV, whereas the optimum rotor diameters for IEC wind class II were found to be essentially the same as the baseline value. Larger rotor diameters were selected for the case of neglecting the impact of the rotor design on the turbine cost, as the increasing AEP was found to be more beneficial in that case. Therefore, the rotor diameter seems to be more related to the wind regime than $c_{l,\max}$.

3.3 Additional Remarks. As indicated by the results, the effect of $c_{l,\max}$ on COE is small over the $c_{l,\max}$ range considered in this study. From the trends in the results, however, increasing $c_{l,\max}$ beyond a value of 1.2 is likely to yield larger reductions in COE, given that gentle stall characteristics can be preserved. Furthermore, the need for higher $c_{l,\max}$ is likely to become more important for wind turbines having a larger rating than 750 kW.

To limit the length of this paper, the optimized twist distributions and pitch settings were not presented because they were not needed to explain the results. Based on the nature of the synthesized airfoil data described in subsection 2.5, the optimized twist distributions and pitch settings were similar for all cases. The twist distributions were smooth and the blade pitch, defined at 75%, radius was between 0 and 4 degrees. Also, the total installed cost of the turbines was between $600 and $900 per kW.

4 Conclusions

The results of this study on the blade design trade-offs using low-lift airfoils for stall-regulated HAWTs have led to the following conclusions and recommendations.

- For minimum COE, the ultimate flap-bending loads for the hurricane condition drive the design away from increasing the swept area with a reduction in $c_{l,\max}$. Therefore, the swept area does not appear to be related to the $c_{l,\max}$ of the airfoils used.
- Overall, the effect of $c_{l,\max}$ on COE is small and a $c_{l,\max}$ of 1.0 appears to be the lower practical limit for airfoils for stall-regulated HAWTs, unless there are other benefits for choosing lower $c_{l,\max}$, such as for noise considerations.
- Higher $c_{l,\max}$ tip-region airfoils become more desirable as machine size increases.
- Future airfoil designs should seek to increase $c_{l,\max}$ while preserving gentle-stall characteristics.

These conclusions may change for other materials, such as carbon fiber, and for smaller turbines because of Reynolds number effects and more important manufacturing issues, i.e., increasing $c_{l,\max}$ could lead to a chord length that is difficult, if not impossible to manufacture. Also, gentle-stall characteristics have been desirable for stall-regulated HAWTs and should be beneficial for any wind turbine, independent of the strategy used to control peak power. For pitch-regulated turbines that pitch towards feather, the need for gentle stall depends on the ability of the controller to keep the blades out of stall in gusty wind conditions.

Acknowledgments

This work was undertaken with the support of the National Renewable Energy Laboratory under Subcontract No. XAF-5-14076-03 (technical monitor: J. L. Tangler). The authors wish to thank the reviewers for their suggestions, which helped improve the paper. Also, the first author would like to express his gratitude to the following NREL employees for their help during the course of this work: Kirk Pierce, Walt Musial, Gunjit Bir, Marshall Buhl, Brian Parsons, Christof Stork, and Charles (Sandy) Butterfield.

References

Eppler, R., and Somers, D. M., 1980, "A Computer Program for the Design and Analysis of Low-Speed Airfoils, Including Transition," NASA TM 80210.

Fuglsang, P. L., and Madsen, H. A., 1995, "A Design Study of a 1 MW Stall-regulated Rotor," Risø-R-799(EN), Risø National Laboratory, Roskilde, Denmark.

Giguère, P., and Selig, M. S., 1997, "Aerodynamic Blade Design Methods for Horizontal Axis Wind Turbines," 13th Annual Canadian Wind Energy Association Conference and Exhibition, Quebec City, Quebec, Canada.

Hibbs, B., and Radkey, R. L., 1983, "Calculating Rotor Performance with the Revised 'PROP' Computer Code," Horizontal-Axis Wind System Rotor Performance Model Comparison—A Compendium, Wind Energy Research Center, Rockwell International, Rocky Flats Plant, Golden, CO, RFP-3508, UC-60.

Huyer, S. A., Simms, D., and Robinson, M. C., 1996, "Unsteady Aerodynamics Associated with a Horizontal-Axis Wind Turbine," *AIAA Journal*, Vol. 34, No. 7, pp. 1410–1419.

International Electrotechnical Commission, 1998, "IEC 61400-1, Ed. 2: Wind Turbine Generator Systems—Part 1: Safety Requirements," FDIS 1998-12-15.

Mandell, J. F., and Samborsky, D. D., 1997, "DOE/MSU Composite Material

Fatigue Database: Test Methods, Materials, and Analysis," Contractor Report SAND97-3002, Sandia National Laboratories, Albuquerque, NM.

Musial, W., 1999, Private communication.

Petersen, J. T., Madsen, H. A., Björck, A., Enevoldsen, P., Òye, S., Ganander, H., and Winkelaar, D., 1998, "Prediction of Dynamic Loads and Induced Vibrations in Stall," Risò-R-1045(EN), Risò National Laboratory, Roskilde, Denmark.

Selig, M. S., and Tangler, J. L., 1995, "Development and Application of a Multipoint Inverse Design Method for Horizontal Axis Wind Turbines," *Wind Engineering*, Vol. 19, No. 2, pp. 91–105.

Selig, M. S., and Coverstone-Carroll, V. L., 1996, "Application of a Genetic Algorithm to Wind Turbine Design," *ASME Journal of Solar Energy Engineering*, Vol. 118, pp. 22–28.

Somers, D. M., 1997a, "Design and Experimental Results for the S809 Airfoil," NREL-SR-440-6918, National Renewable Energy Laboratory, Golden, CO.

Somers, D. M., 1997b, "Design and Experimental Results for the S814 Airfoil," NREL-SR-440-6919, National Renewable Energy Laboratory, Golden, CO.

Sutherland, H., Beattie, A., Hansche, B., Musial, Walt, Allread, J., Johnson, J., and Summers, M., 1994, "The Application of Non-Destructive Techniques to the Testing of a Wind Turbine Blade," SAND93-1380, Sandia National Laboratories, Albuquerque, New Mexico.

Tangler, J. L., and Somers, D. M., 1985, "Advanced Airfoils for HAWTs," American Wind Energy Association WindPower '85 Conference, San Francisco, CA.

Tangler, J. L., and Somers, D. M., 1987, "Status of the Special-Purpose Airfoil Families," American Wind Energy Association WindPower '87 Conference, San Francisco, CA.

Tangler, J. L., Smith, B., and Jager, D., 1992, "SERI Advanced Wind Turbine Blades," NREL/TP-257-4492, National Renewable Energy Laboratory (formerly the Solar Energy Research Institute), Golden, CO.

Tangler, J. L., Kelley, N., Jager, D., and Smith, B., 1994, "Measured Structural Loads for the Micon 65/13," NREL/TP-442-6062, National Renewable Energy Laboratory, Golden, CO.

Tangler, J. L., and Somers, D. M., 1995, "NREL Airfoil Families for HAWTs," American Wind Energy Association WindPower '95 Conference, Washington, DC.

Tangler, J. L., and Selig, M. S., 1997, "An Evaluation of an Empirical Model for Stall Delay Due to Rotation for HAWT," American Wind Energy Association WindPower '97 Conference, Austin, TX.

Tangler, J. L., and Somers, D. M., 1999, "Effect of Airfoil Thickness and Maximum Lift Coefficient on Roughness Sensitivity," 3rd ASME JSME Joint Fluids Engineering Conference, San Francisco, CA.

Wilson, R. E., and Walker, S. N., 1974, "A FORTRAN Program for the Determination of Performance, Load and Stability Derivatives of Windmills," Department of Mechanical Engineering, Oregon State University, Corvallis, Oregon.